INTERNATIONAL JOURNAL FOR NUMERICAL METHODS IN FLUIDS
Int. J. Numer. Meth. Fluids 2003; **43**:651–671 (DOI: 10.1002/fld.494)

Numerical modelling of the pressure wave propagation in the arterial flow

Giuseppe Pontrelli*,† and Enrico Rossoni

Istituto per le Applicazioni del Calcolo-CNR, Viale del Policlinico, 137-00161 Roma, Italy

SUMMARY

A differential model of blood flow through an arterial vessel is presented. It consists of a one-dimensional model describing the non-linear fluid–wall interaction coupled with a simple lumped parameter model which accounts for outlet boundary conditions. The model includes a local stiffening of the vessel and the wave propagation of disturbances due to prosthetic implantations is also studied. The non-linear problem is solved by a finite-difference method on a staggered grid and some numerical simulations are analysed and discussed. Copyright © 2003 John Wiley & Sons, Ltd.

KEY WORDS: wall–fluid interaction; blood flow; numerical methods; stent

1. INTRODUCTION

The study of the pressure and flow waves along an artery has received much attention in the last decades. Mathematical models predicting dynamical profiles are of interest for the clinicians because the shape of such variables are of diagnostic significance and their anomalies can be used to detect pathological states in vascular system. The beat of the heart and the distensibility of the arterial wall results in the occurrence of waves which propagate through the aorta along the major arteries to the periphery. Our aim is to provide a better insight of the mechanism of propagation, and of the changes in the pressure waveform which occurs as it travels along the arteries due to the non-linear wall–fluid interaction.

Wave propagation in arteries has been investigated experimentally, but *in vivo* studies are difficult, expensive and limited to easily accessible arteries. Theoretical studies and computational modelling offer an attractive method of investigation. Some researches have been carried out on the whole systemic circulation [1] or on parts of the arterial tree [2].

* Correspondence to: G. Pontrelli, Istituto per le Applicazioni del Calcolo-CNR, Viale del Policlinico, 137-00161 Roma, Italy.
† E-mail: pontrelli@iac.rm.cnr.it

Contract/grant sponsor: CNR program Agenzia 2000; contract/grant number: CNRC00A3F1_002, 2001

Received 3 March 2002
Revised 26 November 2002

Some authors have shown that velocity field and damping of waves can be described accurately using a linearly elastic quasi-one-dimensional (1D) model, whereas the vessel viscosity can be considered as a second-order effect [3]. On the other hand, experimental studies indicate that the arterial tissue is viscoelastic and anisotropic [4], and, as shown by numerical simulations, wall viscosity cannot be neglected in time-dependent problems [5].

The dynamics induced by the wall deformability modifies the fluid domain and its boundary conditions, and conversely, the flow field, through the stresses exerted on the wall, induces the wall deformation. A feedback effect is generated, and the dynamics of the system is intrinsically coupled (*fluid–structure interaction*). Under the hypothesis that the wave amplitude is small and the wavelength is long compared with the vessel radius, a quasi-1D distributed model is used for the fluid flow. Several models based on pointwise tube laws of type $A = A(p,x)$ have been developed [4]. They do not include any wall displacement along the axial direction due to the shear stress: this can be of some importance when remodelling process and growth of the arterial endothelium are considered. In this work, a 2D linearly viscoelastic membrane in equilibrium with the internal and external forces is presented as a wall model. Because of low mass, the inertia of the wall is negligible compared with the elastic force, and has been ignored. The mathematical description of the phenomenon is given in Section 2.

In the linearized case, the wave propagation is studied by a perturbation analysis on small disturbances in a infinite domain and results as superposition of a forward and a backward travelling waves (Section 3). On the other hand, from a computational point of view, it is necessary to truncate the arterial tree at some level and provide outflow boundary conditions at the truncation points. This can introduce spurious reflections due to a possible impedance mismatch [1]. The problem of assigning the proper boundary conditions to an extracted vessel segment is overcome by coupling it with a Windkessel type model. Despite its simplicity, this is a lumped model predicting the impedance of the termination, as a result of a resistive and a compliant behaviour of the downstream arteries (Section 4). Some numerical results are presented in Section 5 for the unsteady flow sustained by two basic time-dependent forcing, as a benchmark case. The flow dependence on the elasticity and the viscosity parameters is shown. The effect of the elasticity parameter is found to be related to the amplitude of oscillations, while the influence of viscosity parameter is to attenuate the high frequency pulsations in the transient, to reduce the tendency of shock formation as in a purely elastic wall model, and to counterbalance possible instability phenomena. Finally, the case of a varying elastic coefficient (i.e. due to a stent insertion) on the flow dynamics is examined in Section 6.

2. MATHEMATICAL FORMULATION

2.1. The flow equations

Owing to the small deformations of the vascular wall and to the unidirectional nature of blood flow in the arterial tree, a quasi-1D model is adopted. Let us consider a homogeneous fluid of density ρ flowing in an axisymmetric distensible tube of circular cross-section and let us

introduce a set of non-dimensional variables:

$$x \to \frac{x}{R_0}, \quad R \to \frac{R}{R_0}, \quad t \to \frac{tU_0}{R_0}$$
$$u \to \frac{u}{U_0}, \quad p \to \frac{p}{\rho U_0^2}$$

where x is the axial co-ordinate, R is the radius (with R_0 a reference radius), u is the axial velocity, p the transmural pressure, both averaged over the cross-section (with U_0 a characteristic velocity), and t denotes the time.

Let us consider the 1D cross-averaged momentum equation:

$$\frac{\partial u}{\partial t} + u\frac{\partial u}{\partial x} = -\frac{\partial p}{\partial x} + f \tag{1}$$

where f is a viscous term [4]. This is approximated by the friction term of the Poiseuille steady flow in a tube of radius R given by

$$f \simeq -\frac{8u}{Re\,R^2} \tag{2}$$

with $Re = \rho U_0 R_0/\mu$ the Reynolds number and μ the fluid viscosity. As a consequence, the wall shear stress is given by

$$\tau = \left.\frac{\mathrm{d}u}{\mathrm{d}r}\right|_R \simeq -\frac{4u}{Re\,R} \tag{3}$$

Strictly speaking, expressions (2) and (3) hold for a steady flow in a rigid tube, but they are considered acceptable for quasi-steady flows and for small deformations ($R \approx R_0$) [3].

The principle of conservation of mass in a deformable tube is expressed by the following the continuity equation [3]:

$$\frac{\partial R}{\partial t} + \frac{R}{2}\frac{\partial u}{\partial x} + u\frac{\partial R}{\partial x} = 0 \tag{4}$$

2.2. The wall equations

The adequate mechanical characterization of blood vessels is an important prerequisite for a quantitative description of blood flow, mostly in wave propagation phenomena. The properties of vascular tissues are highly non-linear, and many models have been developed for modelling the arterial wall dynamics in physiological and pathological conditions [6]. On the other hand, in a normally stressed vessel the radial deformation around the equilibrium configuration is quite small (typically it does not exceed 10%) and a linear strain–stress law around it is likely to be used. The longitudinal deformation, even smaller and negligible at first approximation, is revealed to be of some importance in the analysis of the wall shear stress and has interest in the investigation of pathological conditions.

Many authors have pointed out the importance of viscoelasticity in modelling arterial walls. Patel and Vaishnav verified the existence of the arterial viscoelasticity through a dynamical experiment [7]. Reuderink *et al.* found that neglecting viscoelasticity generates an underestimation of both phase velocity and damping [3]. Generally, a viscoelastic wall model yields

numerical results closer to measurements than an elastic one, and a dissipative wall is more effective than a viscous fluid in eliminating the high frequency oscillations. The damping resulting from viscoelasticity inhibits sharp peaks of the pressure and of flow pulses and leads to more realistic results when a comparison with experimental data is carried out [5].

For a simpler analysis, we adopted a linear viscoelastic 2D model, given by the following strain–stress relationship:

$$\begin{aligned} T_1(\lambda_1,\lambda_2,\dot{\lambda}_1,\dot{\lambda}_2) &= K\left(\lambda_1+\frac{\lambda_2}{2}-\frac{3}{2}\right)+\gamma\left(\dot{\lambda}_1+\frac{\dot{\lambda}_2}{2}\right) \\ T_2(\lambda_1,\lambda_2,\dot{\lambda}_1,\dot{\lambda}_2) &= K\left(\lambda_2+\frac{\lambda_1}{2}-\frac{3}{2}\right)+\gamma\left(\dot{\lambda}_2+\frac{\dot{\lambda}_1}{2}\right) \end{aligned} \tag{5}$$

where T_1 and T_2 are the non-dimensional stresses in the axial and circumferential direction, λ_1, λ_2 are the principal deformation ratios (see below), $K>0$ is an elasticity coefficient,[‡] $\gamma>0$ is a non-dimensional wall viscosity coefficient and the dot denotes time derivative [5, 8]. The former relations hold in the case of an incompressible and isotropic material, wherein principal directions of strain and stress coincide and express the property that the instantaneous Young's modulus increases with the strain, though by a different amount in the two directions [6].

The simple functional dependence strain–stress in Equations (5) takes into account the viscous effects of a material in time-dependent motions and models the response of the arterial wall to the deformation and to the rate of deformation. The linear form (5) allows a simpler analysis and helps to separate out the contribution of the elastic and viscous parts.

Let us now consider the vessel wall modelled as an elastic axisymmetric membrane. This is a 2D thin shell with a mass negligible compared with that of the fluid contained in it. The membrane, which has no bending stiffness, is capable to deform under the forces exerted by the fluid (i.e. the shear stress τ and the transmural pressure p-cf. (3)) and reaches an equilibrium state. Let $(x_P(s), r_P(s))$ be the Lagrangian co-ordinates of a particle P with s a parametric co-ordinate along the membrane in its symmetry plane. In such reference frame, the principal deformation ratios in the meridional and circumferential directions are, respectively,

$$\lambda_1=\sqrt{\left(\frac{\mathrm{d}r_P}{\mathrm{d}s}\right)^2+\left(\frac{\mathrm{d}x_P}{\mathrm{d}s}\right)^2}, \qquad \lambda_2=\frac{r_P}{R^*} \tag{6}$$

where R^* is the undeformed radius (corresponding to the zero transmural pressure).

Since the fluid equations are expressed in Eulerian co-ordinates, let us operate a transformation of co-ordinate and let us indicate by $R(x,t)$ and $S(x,t)$ the Eulerian counterparts of the Lagrangian co-ordinates of a particle of the membrane. In other words, the position of the point P on the wall that deforms radially and axially is described by the two variables $R(x,t)$ and $S(x,t)$ (see Reference [8]). In such co-ordinate system, the stretch ratios (6) are

[‡] K corresponds to the non-dimensional combination $Eh/\rho R_0 U_0^2$, with E being the Young modulus and h the undeformed arterial thickness.

written as

$$\lambda_1 = \sqrt{\frac{1+R'^2}{S'^2}}, \qquad \lambda_2 = \frac{R}{R^*} \tag{7}$$

(the prime denotes x-derivative). By balance of forces, the fluid–membrane equilibrium equations in tangential and normal directions are provided [9]:

$$R'(T_1 - T_2) + RT_1' = \tau R(1+R'^2)^{1/2} \tag{8a}$$

$$\frac{-R''}{(1+R'^2)^{3/2}} T_1 + \frac{1}{R(1+R'^2)^{1/2}} T_2 = p \tag{8b}$$

3. ANALYSIS OF THE LINEARIZED SYSTEM

Because of the complexity of the mathematical model, we proceed to a preliminary analysis by using a perturbation expansion in an infinite domain. This idealized case will be useful to better understand the nature of the differential problem. When a tube filled with a liquid at rest or flowing with constant velocity is disturbed at one place, the disturbance will be propagated as a wave along the tube at finite speed. For simplicity, let us take a constant equilibrium unstressed state $(R^*, S^*, p^* \equiv 0, u^*)$ as reference configuration[§] and let us perturb the system with infinitesimal quantities $(\tilde{R}, \tilde{S}, \tilde{p}, \tilde{u})$:

$$R = R^* + \tilde{R}, \quad S = S^* + \tilde{S}, \qquad p = 0 + \tilde{p}, \qquad u = u^* + \tilde{u} \tag{9}$$

In the hypothesis of waves of small amplitude and long wavelength, let us also assume that $\tilde{R}', \tilde{R}'', \tilde{S}', \tilde{u}_x, \tilde{p}_x$ and their time derivatives are infinitesimal of the same order.

By neglecting second-order infinitesimals, we have the following approximations (see (7)):

$$\begin{aligned} \sqrt{1+\tilde{R}'^2} &\approx 1 + \frac{\tilde{R}'^2}{2} \approx 1 \\ \lambda_1 &= \sqrt{\frac{1+\tilde{R}'^2}{(1+\tilde{S}')^2}} \approx \frac{1}{1+\tilde{S}'} \approx 1 - \tilde{S}', \qquad \lambda_2 = \frac{R^* + \tilde{R}}{R^*} = 1 + \frac{\tilde{R}}{R^*} \end{aligned} \tag{10}$$

By replacing (9) in Equations (8a), (8b), (1), (4) we obtain

$$K\tilde{R}'\left(\frac{\lambda_1 - \lambda_2}{2}\right) + \gamma\tilde{R}'\left(\frac{\dot{\lambda}_1 - \dot{\lambda}_2}{2}\right) + KR\left(\lambda_1' + \frac{\lambda_2'}{2}\right) + \gamma R\left(\dot{\lambda}_1' + \frac{\dot{\lambda}_2'}{2}\right) = \tilde{\tau}R$$

$$-K\tilde{R}''\left(\lambda_1 + \frac{\lambda_2}{2} - \frac{3}{2}\right) - \gamma\tilde{R}''\left(\dot{\lambda}_1 + \frac{\dot{\lambda}_2}{2}\right) + \frac{K}{R}\left(\lambda_2 + \frac{\lambda_1}{2} - \frac{3}{2}\right) + \frac{\gamma}{R}\left(\dot{\lambda}_2 + \frac{\dot{\lambda}_1}{2}\right) = \tilde{p}$$

[§] For a inviscid fluid, any u^* satisfy the flow equation and its value is irrelevant for the following analysis. For a viscous fluid, $u^* = 0$.

$$\tilde{u}_t + (u^* + \tilde{u})\tilde{u}_x = -\tilde{p}_x + f(\tilde{u})$$

$$\tilde{R}_t + \frac{R^* + \tilde{R}}{2}\tilde{u}_x + (u^* + \tilde{u})\tilde{R}_x = 0$$

The first two terms in the first two equations are infinitesimal of second-order and will be omitted. Thus, after integration (along x) of the first equation, the four equations reduce to

$$K\left(\lambda_1 + \frac{\lambda_2}{2} - \frac{3}{2}\right) + \gamma\left(\dot{\lambda}_1 + \frac{\dot{\lambda}_2}{2}\right) = \int \tilde{\tau}\,\mathrm{d}x \equiv g(\tilde{u}) \tag{11}$$

$$K\left(\lambda_2 + \frac{\lambda_1}{2} - \frac{3}{2}\right) + \gamma\left(\dot{\lambda}_2 + \frac{\dot{\lambda}_1}{2}\right) = \tilde{p}R^* \tag{12}$$

$$\tilde{u}_t + u^*\tilde{u}_x = -\tilde{p}_x + f(\tilde{u}) \tag{13}$$

$$\tilde{R}_t + \frac{R^*}{2}\tilde{u}_x + u^*\tilde{R}_x = 0 \tag{14}$$

The integration of the latter equations is accomplished in two steps: by first solving the wall configuration equations (11)–(12) and then by updating the flow field equations (13)–(14).

3.1. *Wall equilibrium configuration*

Let us suppose the flow variables are known at a certain time. After substitution of (10), the previous two first equations become

$$K\left(\frac{\tilde{R}}{2R^*} - \tilde{S}'\right) + \gamma\left(\frac{\dot{\tilde{R}}}{2R^*} - \dot{\tilde{S}}'\right) = g(\tilde{u}) \tag{15}$$

$$K\left(\frac{\tilde{R}}{R^*} - \frac{\tilde{S}'}{2}\right) + \gamma\left(\frac{\dot{\tilde{R}}}{R^*} - \frac{\dot{\tilde{S}}'}{2}\right) = \tilde{p}R^* \tag{16}$$

Case $\gamma = 0$ (*Purely elastic wall*): The two O.D.E's (15)–(16) become algebraic equations:

$$K\left(\frac{\tilde{R}}{2R^*} - \tilde{S}'\right) = g(\tilde{u}) \tag{17}$$

$$K\left(\frac{\tilde{R}}{R^*} - \frac{\tilde{S}'}{2}\right) = \tilde{p}R^* \tag{18}$$

and solving with respect to $\tilde{R}$ and $\tilde{S}'$ we get

$$\tilde{R} = \frac{2R^*(2\tilde{p}R^* - g(\tilde{u}))}{3K} \tag{19a}$$

$$\tilde{S}' = \frac{2(\tilde{p}R^* - 2g(\tilde{u}))}{3K} \tag{19b}$$

The value of the perturbed deformations are inversely proportional to K and do not depend on $\tilde{p}$ and $g(\tilde{u})$ only, but also on the unstressed value R^*. For an inviscid fluid, we have $g(\tilde{u}) = 0$ and $\tilde{R}/R^* = 2\tilde{S}' = 4\tilde{p}R^*/3K$.

Case $\gamma > 0$ (*Viscoelastic wall*): From (15)–(16) we have

$$\dot{\tilde{R}} = -\frac{K}{\gamma}\tilde{R} + \frac{2R^*(2\tilde{p}R^* - g(\tilde{u}))}{3\gamma}, \qquad \dot{\tilde{S}}' = -\frac{K}{\gamma}\tilde{S}' + \frac{2(\tilde{p}R^* - 2g(\tilde{u}))}{3\gamma} \tag{20}$$

The general integral of this system is a solution of exponential type $e^{-\sigma t}$ with damping factor $\sigma = K/\gamma > 0$. When $K \gg \gamma$, the damping factor is large and the solution is rapidly decaying to the asymptotic values given by (19). If γ is comparable with K the transient time can be relevant.

3.2. Flow field

Once the wall configuration is computed at a given time, the fluid dynamics variables are updated as follows. For the sake of simplicity, we concern ourselves with the purely elastic case and let us assume that the viscous resistance is negligible ($f(\tilde{u}) = g(\tilde{u}) = 0$). By replacing expression (19a) into (13)–(14) we get the first-order linear system:

$$\tilde{u}_t + u^*\tilde{u}_x + \tilde{p}_x = 0$$

$$\tilde{p}_t + \frac{3K}{8R^*}\tilde{u}_x + u^*\tilde{p}_x = 0$$

that is

$$\mathbf{w}_t + \mathbf{A}\mathbf{w}_x = \mathbf{0} \tag{21}$$

where

$$\mathbf{w} = \begin{pmatrix} \tilde{u} \\ \tilde{p} \end{pmatrix}, \quad \mathbf{A} = \begin{pmatrix} u^* & 1 \\ \dfrac{3K}{8R^*} & u^* \end{pmatrix}$$

The eigenvalues of A:

$$\omega_{1,2} = u^* \pm \frac{1}{2}\sqrt{\frac{3K}{2R^*}}$$

are real and distinct (system of hyperbolic type) and the characteristics are the straight lines:

$$\frac{\mathrm{d}x_1}{\mathrm{d}t} = \omega_1 = u^* + c, \qquad \frac{\mathrm{d}x_2}{\mathrm{d}t} = \omega_2 = u^* - c \tag{22}$$

with

$$c = \frac{1}{2}\sqrt{\frac{3K}{2R^*}} > 0 \tag{23}$$

Since in physiological regimes $u^* \ll c$ (subcritical flow), the characteristics have opposite signs. System (21) can be put in normal form as follows. By defining

$$\mathbf{T} = \begin{pmatrix} c & 1 \\ -c & 1 \end{pmatrix}, \quad \mathbf{\Lambda} = \mathrm{diag}(\lambda_1, \lambda_2) = \begin{pmatrix} u^* + c & 0 \\ 0 & u^* - c \end{pmatrix}$$

we have

$$\mathbf{TA} = \mathbf{\Lambda T}$$

Let be $\mathbf{W} = \mathbf{Tw}$. We have

$$\mathbf{W}_t + \mathbf{\Lambda W}_x = \mathbf{0} \tag{24}$$

or, in scalar form

$$(\tilde{p} + c\tilde{u})_t + (u^* + c)(\tilde{p} + c\tilde{u})_x = 0$$

$$(\tilde{p} - c\tilde{u})_t + (u^* - c)(\tilde{p} - c\tilde{u})_x = 0$$

$W_1 = \tilde{p} + c\tilde{u}$ and $W_2 = \tilde{p} - c\tilde{u}$ are the two Riemann invariants of the hyperbolic system (24): they do not vary along the characteristic lines (22) and concur to the formation of the pressure and flow pulses. The resulting solution is given by linear superposition of a progressive and of a regressive wave, with finite speeds $u^* + c > 0$ and $u^* - c < 0$, respectively [10].

The general solution of system (24) in terms of $\tilde{p}$ and $\tilde{u}$ is given by

$$\tilde{p} = \frac{W_1 + W_2}{2} = \frac{\phi(x - (u^* + c)t) + \psi(x - (u^* - c)t)}{2}$$

$$\tilde{u} = \frac{W_1 - W_2}{2c} = \frac{\phi(x - (u^* + c)t) - \psi(x - (u^* - c)t)}{2c}$$

where ϕ and ψ are two arbitrary differentiable functions depending on the initial data.

Note that the linear elastic theory (in absence of longitudinal stress and strain) predicts a different non-dimensional speed given by the $c_{\mathrm{MK}} = (1/U_0)\sqrt{Eh/2\rho R_0 R^*} = \sqrt{K/2R^*}$ (Moens–Korteweg formula).

A general analysis with similar arguments would be carried out when the perturbation is around a reference (i.e. *pre-stressed*) state different from the unstressed configuration.

4. BOUNDARY CONDITIONS

Equations (1), (4) and (8), together with the constitutive equations (5), model the non-linear fluid–wall interaction and are solved in the segment between the two points $x = 0$ (proximal end) and $x = L$ (distal end) which constitute the fictitious boundaries of the differential

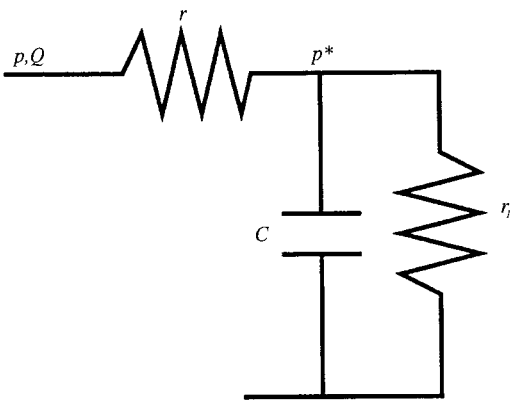

Figure 1. The Westkessel model described by Equations (26) and (27).

problem. According to the considerations of Section 3, we would need to prescribe the characteristic variable W_1 on the proximal end and W_2 on the distal end as boundary conditions. Under some restrictions, alternative boundary conditions can also be expressed in terms of the primitive variables u and p, or with a functional relation between them [11].

As a matter of fact, the analysis carried out on a linearized system was derived in the hypothesis of infinitesimal perturbations around an unperturbed configuration. In the non-linear case and under a finite load $\bar{p}$, the arterial fluid–wall dynamics is more complex and another approach for the boundary prescription will be proposed here. The possibility to incorporate a 1D model in a full lumped parameter model based on the electrical circuit analogue is presented by Formaggia *et al.* [12] and gives account for a global balance of flow and pressures in the cardiovascular network (*multiscale approach*). In such a case the matching interface condition between systems of different physical dimension is carefully addressed. However, to investigate the response of an arterial segment to a given pressure pulse, a relatively simpler method is likely to be used. An arbitrary pulsatile boundary condition on the pressure

$$p(0,t) = f(t) \tag{25}$$

is given at the inlet for a specific form of f, see Section 5. An outflow condition of type (25) is not realistic, since the peripherical termination influences the response of the vessel and a feedback effect has to be considered. Following the idea of other authors, a Windkessel type model is coupled as a distal load, in order to account for the remaining terminal vascular system beyond the end of the vessel [2, 13, 14]. Based again on the electrical analogue circuit, the three-elements Windkessel (also called the *Westkessel model*) (WK) consists in a resistance in series with a parallel combination of a resistance and a capacitor [14] (see Figure 1). This is described by the following two equations:

$$p - p^* = rQ \tag{26}$$

$$Q = C\frac{\mathrm{d}p^*}{\mathrm{d}t} + \frac{p^*}{r_1} \tag{27}$$

where $r + r_1$ is the total peripherical resistance, C the total compliance, r the characteristic impedance, p^* is the pressure downstream of the vessel and $Q = \pi R^2 u$ is the flow rate. By eliminating p^* from Equations (26)–(27) we get

$$F_{\mathrm{WK}}(p, \dot{p}, Q, \dot{Q}) = \frac{p}{r_1} + C\frac{\mathrm{d}p}{\mathrm{d}t} - Cr\frac{\mathrm{d}Q}{\mathrm{d}t} - \frac{r + r_1}{r_1}Q = 0 \tag{28}$$

that give a differential relation between p and Q (or u) to be imposed at the outlet. The boundary condition (28) is based on a lumped relation between flow and pressure in the smaller arteries and arterioles and can be read, to some extent, as a differential condition of a Riemann invariant W_2 (see Section 3). It does not include spatial distribution of the network of smaller arteries and is not able to capture the wave propagation phenomena. Nevertheless, provided a correct estimation of the three parameters C, r, r_1 is given, it models the physical phase lag between flow and pressure and avoids spurious reflections present in other models [15].

Finally, the boundary conditions for R are given by considering a *infinitely long* vessel[¶] with free ends. Therefore, the conditions

$$R' = R'' = 0, \qquad S' = 1 \tag{29}$$

hold at the ends.[‖] From (8b) it follows that the implicit relation for R:

$$Rp = T_2$$

(*law of Laplace*) unifies the three conditions (29) and is prescribed at the boundaries.

Moreover, the boundary conditions on S:

$$S(0, t) = 0, \qquad S(L, t) = L^*$$

expressing a finite axial displacement L^* is imposed.

The initial condition is chosen by considering the equilibrium configuration obtained with a constant input pressure. Then the system is left evolving forced by pressure (25).

5. NUMERICAL APPROXIMATION AND COMPUTATIONAL RESULTS

Equations (1)–(4)–(8)–(5) are solved numerically in a fully coupled way in a finite interval $[0, L]$. Let us consider a sequence of $n + 1$ equispaced grid points of co-ordinates $(x_i)_{i=0,\ldots,n}$ with $x_0 = 0$ and $x_n = L$. The spatial discretization is obtained by evaluating membrane stresses, strains and their time derivatives (see Equation (5)) at n inner points $\xi_i = (x_i + x_{i+1})/2$ of a staggered grid by considering averaged neighbouring variables. On the other hand, wall–fluid equilibrium equations (8) and fluid equations (1)–(4) are computed at the $n - 1$ inner points x_i. The first derivatives are approximated by a centred finite-difference scheme and the resulting non-linear system includes (28) as final equation and is solved by a globally convergent Newton type method. The time discretization is based on the second-order Runge–Kutta formula, in such a way the global scheme is of second-order in space and time [16].

[¶] Here *infinitely long* means of length much larger than the reference radius R_0.

[‖] Conditions (29) imply $\lambda_1 = 1$ (null axial stretch ratio), see (7).

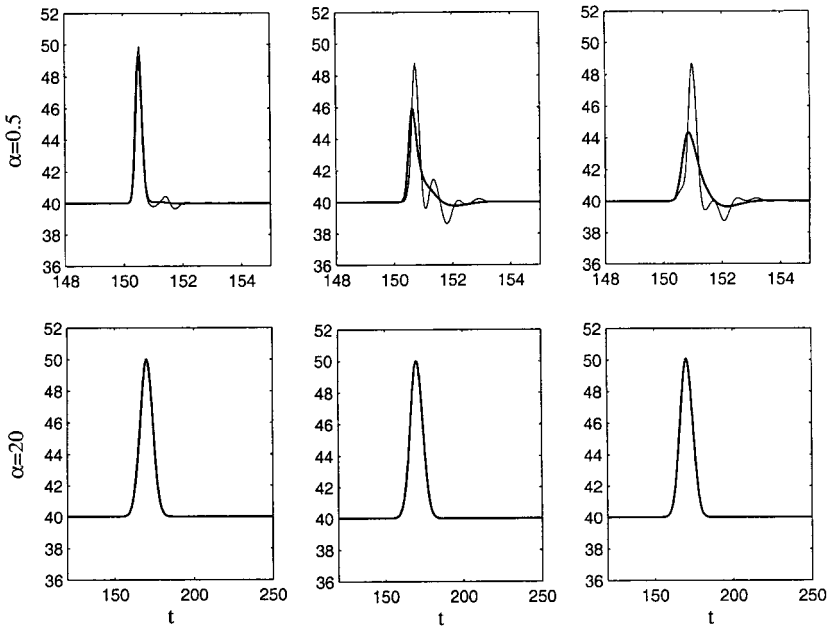

Figure 2. Pressure histories at three locations (left, centre and right) in the vessel. The first row refers to a sharp pulse ($K = 600$—thin line is for $\gamma = 10$, thick line for $\gamma = 100$), the second row to a long pulse (no variation with γ occurs). Note the different time scale.

The following values for the WK model are considered [2, 17]:

$$r = 1 \text{ mmHg s/ml} \quad r_1 = 3.06 \text{ mmHg s/ml} \quad C = 1.06 \text{ ml/mmHg} \tag{30}$$

non-dimensionalized as

$$r \to \frac{rR_0^2}{\rho U_0}, \quad r_1 \to \frac{r_1 R_0^2}{\rho U_0}, \quad C \to \frac{C\rho U_0^2}{R_0^3}$$

The other parameters have been chosen around some typical values to obtain results of physiological interest and varied in a typical range to test the sensitivity of the system to their perturbation. Non-linear models turn out to be very sensitive to the many material parameters which characterize the specific flow problem.

In all the numerical experiments we selected $R^* = 1$, $L = L^* = 8$, $\Delta x = 10^{-2}$ and $\Delta t = 5 \times 10^{-4}$. These values guarantee the numerical stability for the set of parameters considered. The accuracy of the solution is controlled since the solution corresponding to a finer grid does not reveal a different structure or unresolved patterns (grid independence). Since in wave propagation phenomena the dissipative effect of the blood viscosity is a minor effect [4], in the following simulations an inviscid fluid is considered ($f \equiv 0$ in (1) and $\tau = 0$ in (8a)).

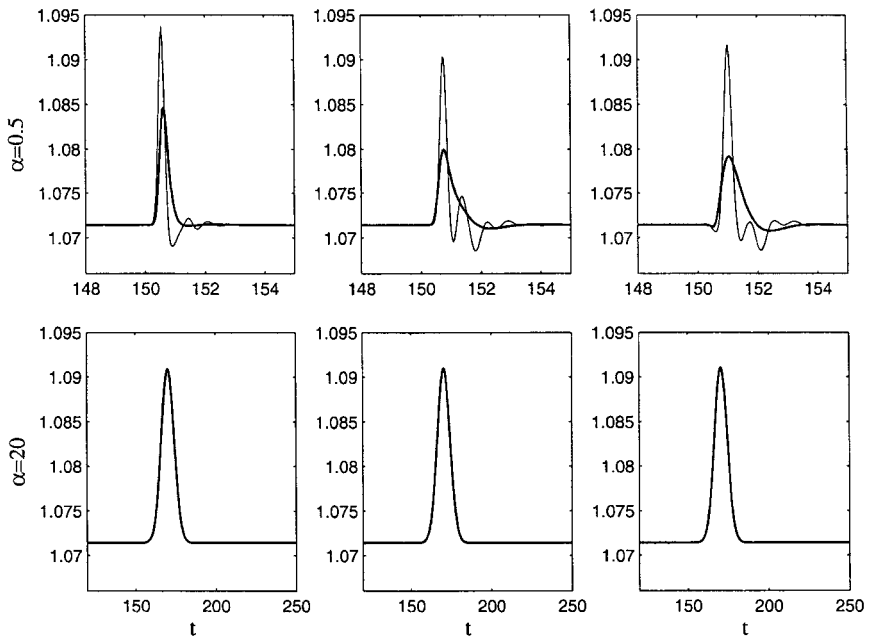

Figure 3. Radial deformation histories at three locations (left, centre and right) in the arterial vessel. The first row refers to a sharp pulse ($K = 600$—thin line is for $\gamma = 10$, thick line for $\gamma = 100$), the second row to a long pulse (no variation with γ occurs). Note the different time scale.

In this fundamental study, the response of the vessel to a pressure input is investigated. This signal can be decomposed by Fourier analysis and represented as a pulse (a dominant harmonic) and a superposition of the other components repeated with some periodicity: hence, the contributions of a single pulse and of a train of waves will be examined separately.

5.1. *Single pressure pulse*

Let us first impose a localized pressure pulse centred in t^*, of half-width α, and amplitude A:

$$p(0,t) = \bar{p} + A \exp\left[-50\left(\frac{t - t^*}{2\alpha}\right)^2\right] \tag{31}$$

Out of the time interval $[t^* - \alpha, t^* + \alpha]$ where the peak is located, the pressure equals the mean pressure $\bar{p}$. The following values have been fixed as:**

$$\bar{p} = 40, \quad A = 10 \tag{32}$$

and $K = 600$ has been taken as elastic parameter. Actually, the values of K and $\bar{p}$ are not independent, being the mean deformation in relation with the ratio $\bar{p}/K$: it turns out that for

** The values of the non-dimensional parameters are defined by letting: $R_0 = 0.5$ cm, $U_0 = 50$ cm/s, $T_0 = 1$ s and with a mean pressure of 75 mmHg.

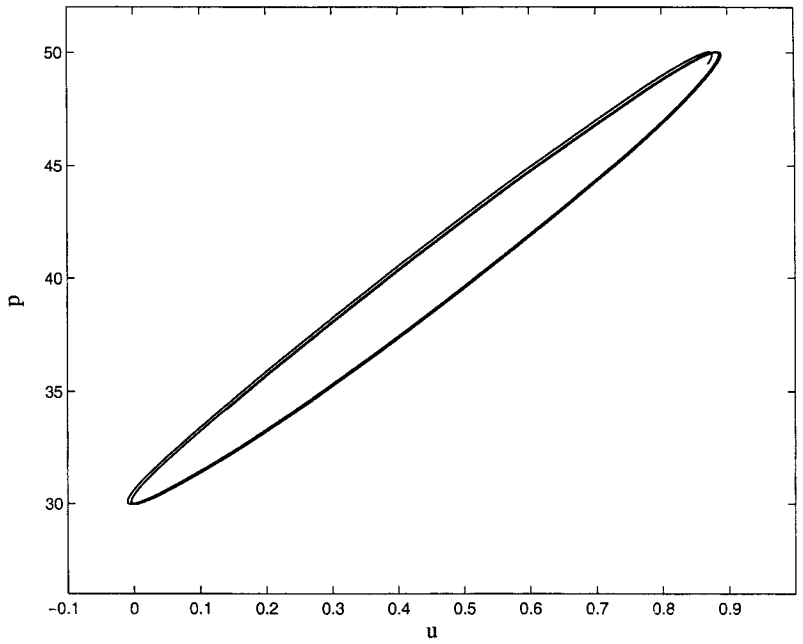

Figure 4. Pressure versus flow velocity in the centre point over more than one cycle. The eccentricity of the hysteresis curve depends on the WK model parameters. The WK values used in the simulation are reported in (30).

$\bar{p}/K < \simeq 0.01$ the wall increases its stiffness and the numerical problem becomes harder. On the other hand, for a value of $\bar{p}/K$ too large, the system undergoes an unrealistic deformation and the present model is not physically admissible.

A sequence of simulations showed that the propagation phenomenon is critically dependent on the sharpness of the pulse, that is the value of α. For α small (i.e. $\leqslant 1$), corresponding to a sharp peak, the response of the vessel to the impulsed pressure occurs in a short time compared with the characteristic transit time. The pulse is followed by an oscillatory tail after the peak, reduced with the dissipative coefficient γ (see Figures 2 and 3). This spreading of the pulse is due to the natural oscillations of the membrane which have a comparable frequency and, at low wall viscosity, are excited. More significantly, the character of the propagation is greatly influenced by the values of the termination. In particular, the resistances r and r_1 have a strong effect on the onset of the reflections, while the influence of C is much lower. A rigorous procedure requires the tuning of the parameters of the WK model to match impedance with the distributed model. The characterization of the termination model is beyond the scope of this work and can be found elsewhere [13].

A more remarkable case concerns a pulse having a duration comparable with the systolic phase ($\approx 0.4\,\mathrm{s}$). Numerical results for $\alpha \approx 20$ show the impulse propagating undisturbed downstream, with no appreciable damping or dispersion (Figures 2 and 3). The character is of a travelling wave, with pressure and flow out of phase.

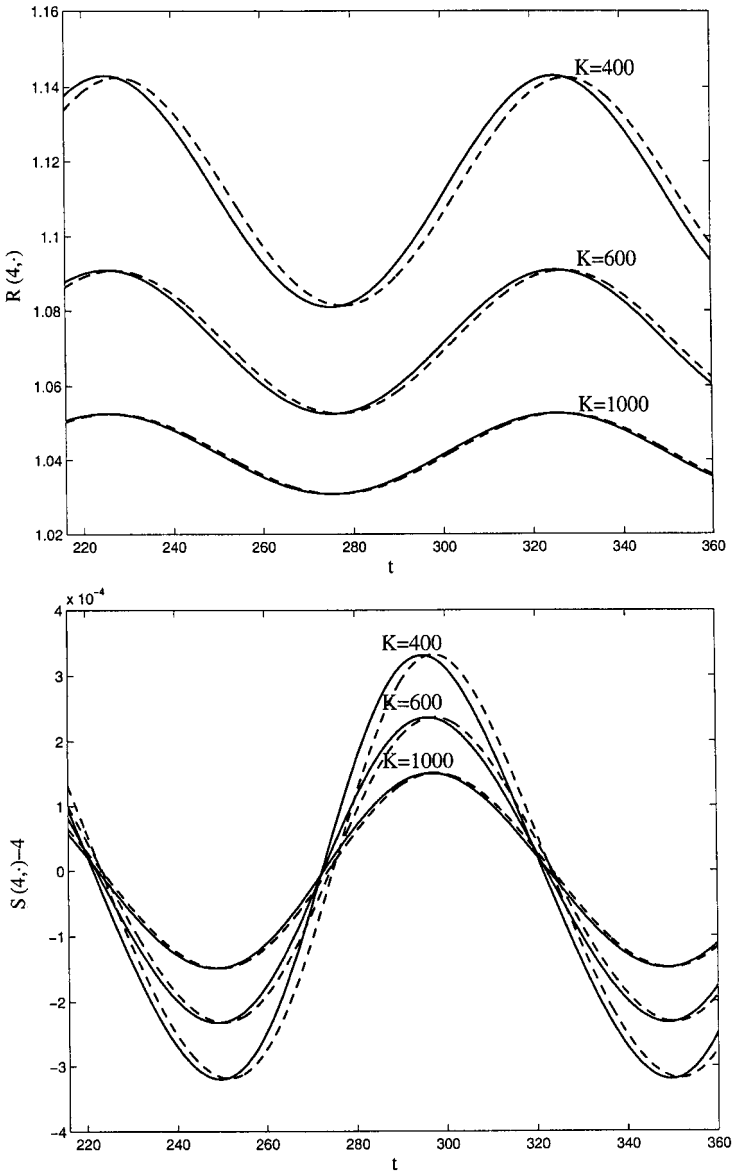

Figure 5. Radial (above) and longitudinal (below) deformations at the centre of the tube for three values of the elasticity coefficient K, in the case of periodic flow. Continuous line is for $\gamma = 10$, dashed line for $\gamma = 1000$.

The wave speed has been determined as in experiments: the transit time of the peak of the pressure pulse has been measured over a known distance. The main difficulty is that the wave changes in shape as it travels, and it is difficult to keep a single reference value for the full wave. Moreover, in a vessel of finite length, the wave speed may depend on the point where

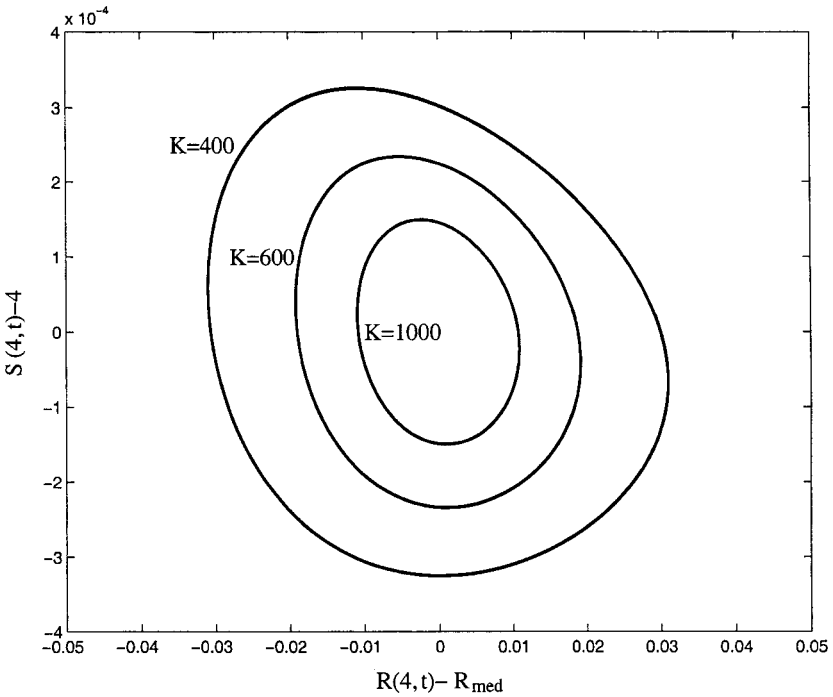

Figure 6. Plot of R versus S of a particle around the centre of oscillation R_{med} in a time cycle. Note the different scale of the deformation.

it is measured and the change in shape is associated with reflections from the boundaries. The apparent measured wave speed may not correspond to the wave speed of a wave travelling in an infinite tube with the same viscoelastic properties (see Section 3 (23)). See Section 6 for comparative results.

5.2. *Train of sine waves*

As a periodic forcing, an oscillatory pressure with a more realistic frequency is assigned at the inlet:

$$p(0,t) = \bar{p} + A\sin(2\pi S_t t) \tag{33}$$

and $S_t = R_0/U_0T_0$ is the Strouhal number with T_0 the period of the incoming wave. The values of $\bar{p}$ and A are as in (32), and $S_t = 0.01$ in agreement with the physiological values. To avoid the effect of the initial conditions, in the numerical simulations the transient has been dropped and only the solution after the second period is considered.

The persistence of sinusoidal oscillations over the mean values occurs with the same input frequency S_t and with amplitudes depending on the elasticity parameter (see below), while the length of the wave does not change with K and γ. A small phase shift between p and u is evidenced from the hysteresis loop depicted in Figure 4. The eccentricity is much smaller

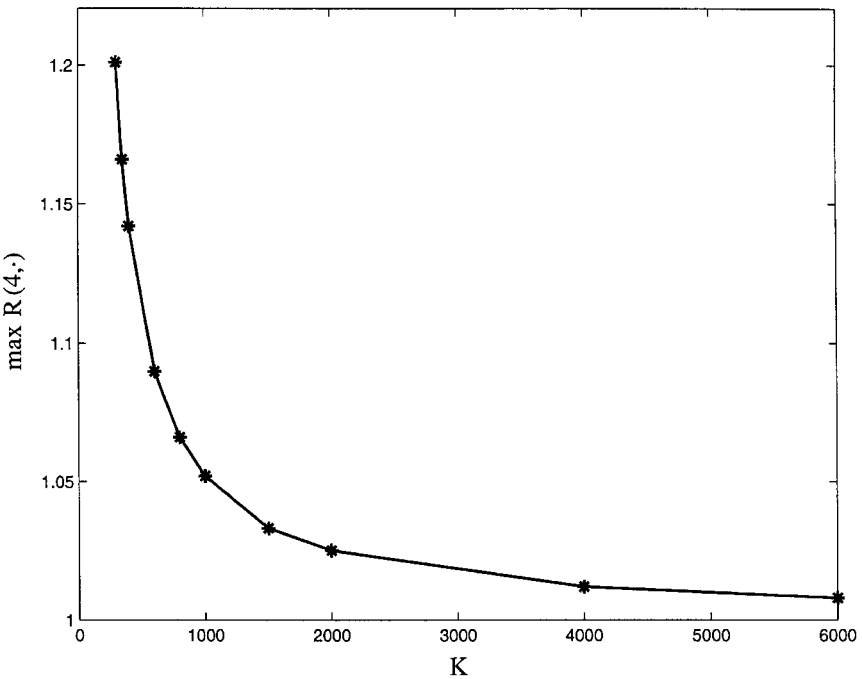

Figure 7. The maximum radial deformation at the centre of the tube at different elasticity coefficients K. Starred points are results from simulations, continuous curves are obtained by a linear interpolation.

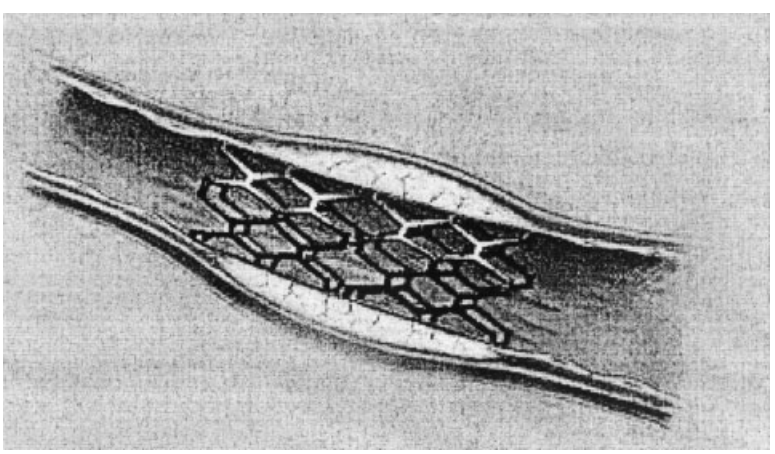

Figure 8. Implantation of a stent in a stenotic artery.

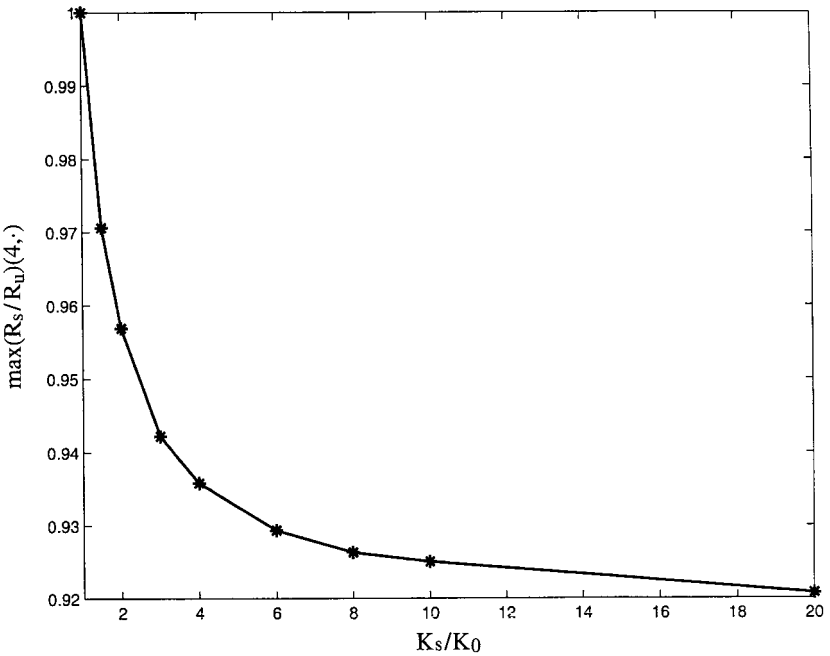

Figure 9. Behaviour of the ratio between the stented and the unstented maximum deformation at the centre of the stented artery with K_s/K_0 ($K_0 = 600, \sigma = 2$). The ratio tends asymptotically to the value for the rigid tube.

than 1 and depends again on the values of the WK model, but not on the viscoelasticity parameters K and γ. This hysteresis curves neither depend on the point along the tube and this proves that no reflection is present at such frequency.

The viscosity of the wall, parametrized by γ, is expected to give an attenuation of the wave profiles, but its effect depends on the magnitude of the strain rates: the viscous damping affects only waves of relatively short length such as those of the wall natural oscillation [5, 15] or sharp pulses, but is irrelevant for the long wavelength typical of the vascular system. A large value of γ ($\approx 10^3$) would slightly shift the profiles, but not the wave amplitude (Figure 5). Since γ multiplies strain rates that are extremely small, the damping influence is felt only for $\gamma \gg 0$ (i.e. 10^6) and, in such a case, a reduction in the amplitude of deformation R is also reported. In the simulations, we fix $\gamma = 10$ and we let vary $350 \leqslant K \leqslant 6000$. The longitudinal deformation S exhibits very small changes compared with the radial one. A much sensible effect of the axial extension and compression would be evident by considering the viscous fluid and its shear stress at the wall. A phase shift of almost $\pi/2$ is clearly visible. The curves S/R in a period of time around the centre of oscillation are depicted in Figure 6. Finally, the dependence of the amplitude of the radial deformation on K is found to be inversely linear (Figure 7). The propagation features correspond to waves travelling along the tube, and the same considerations for the wave speed as in the single pressure pulse case hold.

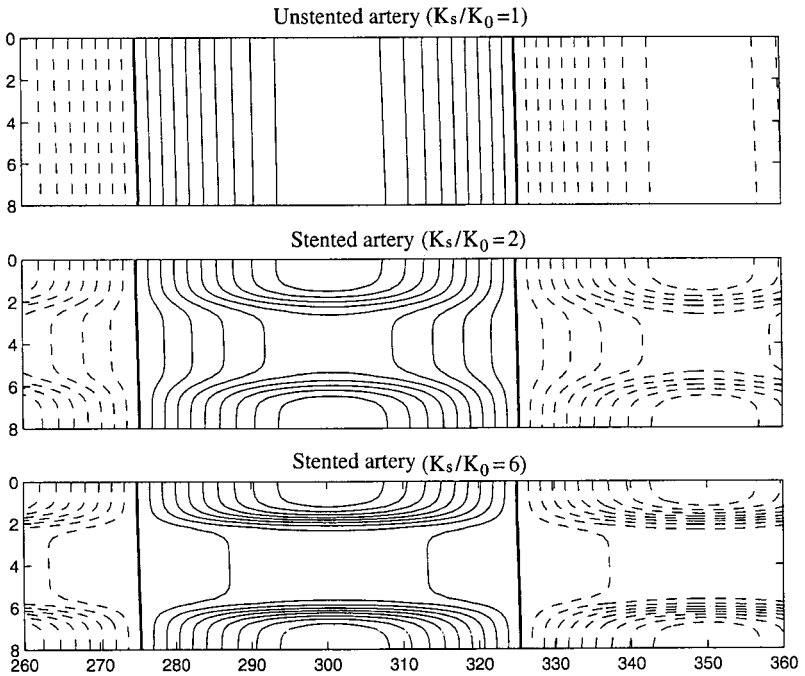

Figure 10. Space–time evolution of the membrane radial velocity in a stented artery for three values of K_s ($K_0 = 600, \sigma = 2$). Thick lines indicates the zero level, continuous lines positive levels, dashed lines negative levels. x-axis is vertical and time axis is horizontal.

6. A CLINICAL APPLICATION: THE STENT INSERTION

In many vascular pathologies, when the arterial lumen is extremely reduced, the stenting methodology is successfully employed since many decades. It is based on the implant of a tubular endoprosthesis (*stent*) to support the arterial wall (Figure 8). Despite its complex geometrical structure and a variety of mechanical characteristics, a stent can be schematically represented with a stiff cylindrical wiremesh placed in the vessel to prevent or to correct narrowing of the section (i.e. stenosis) [18]. Although the stent implantation changes the geometry of the vessel and consequently induces important disturbances in the local flow, a relevant effect in the wall–fluid interaction are the change of the compliance due to the sudden rising of the elasticity coefficient, and the features of the propagation [19].

In an artery of elasticity coefficient K_0, let us consider a stent of length 2σ centred in a point x^* and with elastic parameter $K_s > K_0$. Therefore, the elasticity parameter along the stented artery is subject to an abrupt change given by

$$K(x) = \begin{cases} K_s & \text{if } |x - x^*| < \sigma \\ K_0 & \text{otherwise} \end{cases}$$

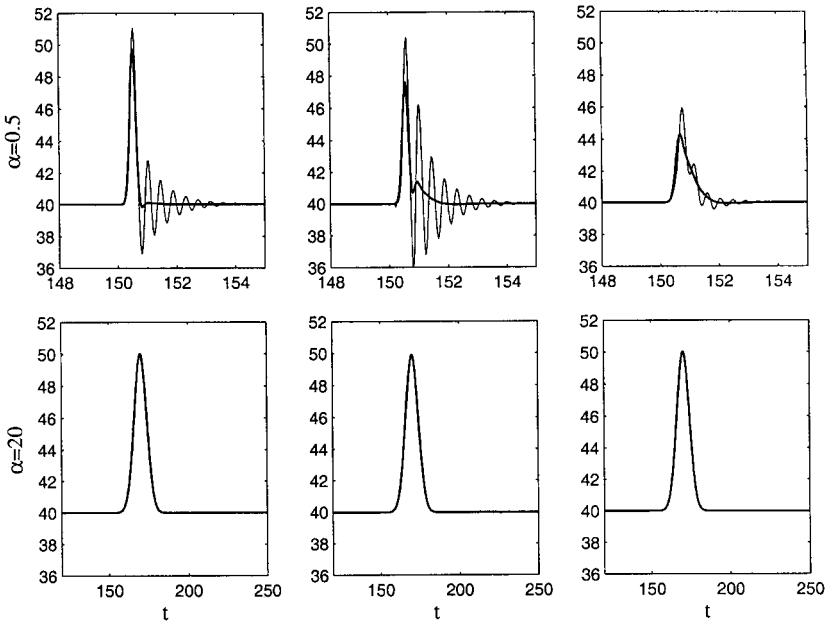

Figure 11. Pressure histories at three locations (left, centre and right) in the stented arterial vessel ($K_0 = 600, K_s = 6000, \sigma = 2$). The first row refers to a sharp pulse (thin line is for $\gamma = 10$, thick line for $\gamma = 100$), the second row to a long pulse (no variation with γ occurs). Note the different time scale and compare with Figure 2.

but, to avoid a compliance mismatch between the relatively rigid stented segment and the distensible vessel, the elastic parameter is modelled by a continuous rapidly changing function:

$$K(x) = K_0(1 + \delta e^{-((x-x^*)/\sigma)^8}), \qquad \delta = \frac{K_s - K_0}{K_0} \tag{34}$$

(for $K_s = K_0$ a uniform elasticity coefficient is recovered). The effect of a physiological local hardening or softening of an artery and the mechanical properties of stents can be also roughly modelled by varying the value of δ and σ.

In the numerical simulations, we fixed $R^* = 1$, $L = L^* = 8$, $x^* = 4$ $\sigma = 2$ (stent two diameters long), $K_0 = 600$ and we varied K_s in (34) up to 12 000, with the wall viscosity coefficient $\gamma = 10$ unchanged.

As expected, the maximum values of the deformation and of the pressure at the centre of the tube are reduced with K_s/K_0, and the asymptotic value of rigid wall is attained (see Figure 9). On the other hand, when subject to the periodical forcing (33), the variation of the elasticity coefficient does not modify the frequency of the oscillation. The space–time evolution of the membrane radial velocity in an unstented and a stented artery are compared in Figure 10. The pressure and radial deformation time histories in three points—upstream the stent, centred in x^*, and downstream the stent—and subject to the impulsed pressure (31) are depicted in Figures 11–12. The reflections due to jump of K at the stent junctions are present when α is small and are reduced or disappear with the wall viscosity.

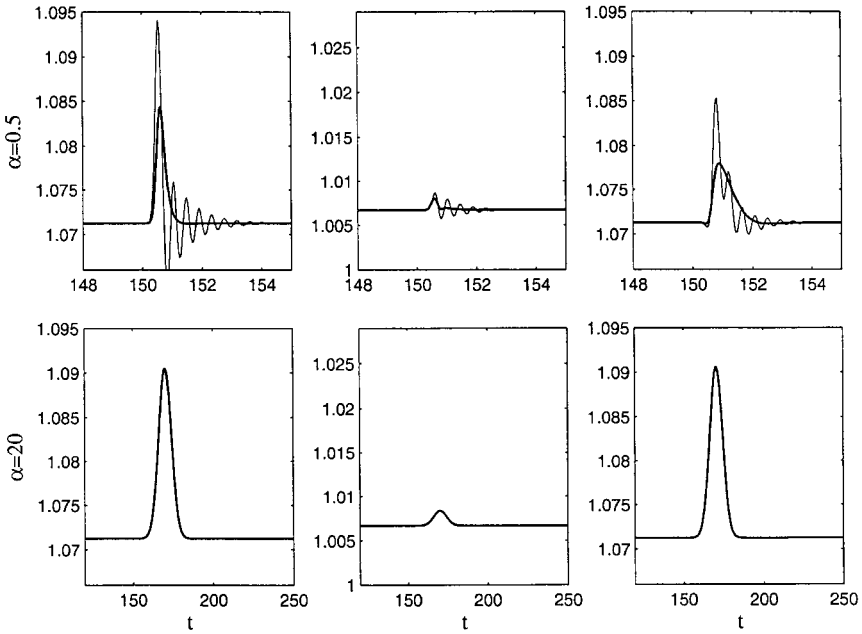

Figure 12. Radial deformation histories at three locations (left, centre and right) in the stented arterial vessel ($K_0 = 600, K_s = 6000, \sigma = 2$). The first row refers to a sharp pulse (thin line is for $\gamma = 10$, thick line for $\gamma = 100$), the second row to a long pulse (no variation with γ occurs). Note the different time scale and compare with Figure 3.

7. CONCLUSIONS AND PERSPECTIVES

The dynamics of the pulsatile flow in an arterial segment has been studied in relation to the viscoelastic properties of the vessel wall. The fluid–wall interaction is described by a 1D model and is expressed by a set of four non-linear partial differential equations plus an ODE describing the peripherical circulation as a lumped parameter model. Although the latter is unable to describe wave propagation phenomena, it is able to absorb the waves travelling in the tube and prevents the non-physical reflections that arise when a Dirichlet type boundary condition is imposed. However, it needs the estimation of three parameters to avoid impedance mismatch.

The hyperbolic nature of propagation phenomenon has been analysed in the linearized case. The dependence on the many parameters has been pointed out in the case of oscillatory flow and the influence of some of them in a case of clinical relevance has been examined. The model can be generalized to account for vessel tapering and bending. Finally, the geometrical, physical and biomechanical parameters need to be carefully identified according to a specific flow problem.

ACKNOWLEDGEMENTS

This work has been partially funded by the CNR program *Agenzia2000*, no. CNRC00A3F1_002, 2001.

REFERENCES

1. Stergiopulos N, Meister JJ, Westerhof N. Evaluation of methods for estimation of total arterial compliance. *American Journal of Physiology* 1995; **268**:H1540–H1548.
2. Raines JK, Jaffrin MY, Shapiro AH. A computer simulation of arterial dynamics in the human leg. *Journal of Biomechanics* 1974; **7**:77–91.
3. Reuderink PJ, Hoogstraten HW, Sipkema P, Hillen B, Westerhof N. Linear and non-linear one-dimensional model of pulse wave transmission at high Womersley numbers. *Journal of Biomechanics* 1989; **22**(8/9):819–827.
4. Fung YC. *Biomechanics*: *Mechanical Properties of Living Tissues* (2nd edn). Springer, New York, 1993.
5. Pontrelli G. A mathematical model of flow in a liquid-filled viscoelastic tube. *Medical and Biological Engineering and Computing* 2002; **40**:550–556.
6. Humphrey J. Mechanics of the arterial wall: review and directions. *Critical Review in Biomedical Engineering* 1995; **23**(1/2):1–162.
7. Patel DJ, Vaishnav RN. *Basic Hemodynamics and its Role in Disease Processes*. University Park Press: Baltimore, 1980.
8. Pedrizzetti G. Fluid flow in a tube with an elastic membrane insertion. *Journal of Fluid Mechanics* 1998; **375**:39–64.
9. Green AE, Adkins JE. *Large Elastic Deformations*. Clarendon Press: Oxford, 1960.
10. Pythoud F, Stergiopulos N, Meister JJ. Forward and backward waves in the arterial system: non-linear separation using Riemann invariants. *Technology and Health Care* 1995; **3**:201–207.
11. Godlewski E, Raviart PA. Numerical approximation of hyperbolic systems of conservations laws. *Applied Mathematical Science*, vol. 118. Springer: New York, 1996.
12. Formaggia L, Nobile F, Quarteroni A, Veneziani A. Multiscale modelling of the circulatory system: a preliminary analysis. *Computing and Visualization in Science* 1999; **2**:75–83.
13. Stergiopulos N, Young DF, Rogge TR. Computer simulation of arterial flow with applications to arterial and aortic stenoses. *Journal of Biomechanics* 1992; **25**:1477–1488.
14. Olufsen M. Structured tree outflow condition for blood flow in larger systemic arteries. *American Journal of Physiology* 1999; **276**:H257–H268.
15. Pontrelli G. Non-linear problems in arterial flows. *Non-linear Analysis*, *Theory*, *Methods & Applications* 2001; **47**:4905–4915.
16. Fletcher CA. *Computational Techniques for Fluid Dynamics*, Springer Series of Computational Physics, vol. 2. Springer: Berlin, 1991.
17. Deswysen B, Charlier AA, Gevers M. Quantitative evaluation of the systemic arterial bed by parameter estimation of a simple model. *Medical and Biological Engineering and Computing* 1980; **18**:153–166.
18. Auricchio F, Di Loreto M, Sacco E. Finite-element analysis of a stenotic artery revascularization through a stent insertion. *Computer Methods in Biomechanics and Biomechanical Engineering* 2001; **4**:249–263.
19. Formaggia L, Nobile F, Quarteroni A. A one dimensional model for blood flow: application to vascular prosthesis. In *Mathematical Modelling and Numerical Simulation in Continuum Mechanics*, Lecture Notes in Computer Science Engineering, vol. 19, Babuska, Miyoshi, Ciarlet (eds). Springer: Berlin, 2002; 137–153.

